Physica A 413 (2014) 544–553

Contents lists available at ScienceDirect

Physica A

journal homepage: www.elsevier.com/locate/physa

Asymmetric transport of passive tracers across heterogeneous porous media

J. Alvarez-Ramirez, F.J. Valdes-Parada, E. Rodriguez, L. Dagdug, L. Inzunza *

División de Ciencias Básicas e Ingeniería, Universidad Autónoma Metropolitana-Iztapalapa, Apartado Postal 55-534, México D.F., 09340, Mexico

HIGHLIGHTS

- Heterogeneous porous media with constant porosity are studied.
- Brownian dynamics simulations were used for studying the diffusion.
- Asymmetrical diffusion across the interface was detected.
- Asymmetries are explained by the advection-like effects at the interface.

ARTICLE INFO

Article history:
Received 21 March 2014
Received in revised form 3 July 2014
Available online 11 July 2014

Keywords:
Heterogeneous porous media
Diffusion
Transport asymmetry
Effective medium equations

ABSTRACT

Experimental results on tracer transport in a porous column consisting of two adjacent segments of different (fine and coarse) glass bead packs having the same porosity value, have shown that the breakthrough curve behavior depends on the transport direction (Berkowitz et al. (2009)). It was found that tracers migrating in the fine-to-coarse (FC) direction arrive significantly faster than in the coarse-to-fine (CF) direction. In this work, we simulate Brownian tracers moving in a 2D random porous medium in a configuration similar to that of the referred experimental set-up. By considering only diffusive effects, the results confirmed the transport asymmetry across the heterogeneous interface. Arguments based on effective medium equations for the porous medium transport indicate that the asymmetry can be explained by subtle differences of effective diffusivity between the coarse and fine porous medium. In turn, such diffusivity differences are induced by differences in the tortuosity and porosity in the vicinity of the porous media boundary.

1. Introduction

Recently, Berkowitz et al. [1] considered the case of tracer dispersive transport in a porous column consisting of two adjacent segments of different (fine and coarse) glass bead packs, but having the same porosity value. A schematized illustration of the porous medium configuration is described in Fig. 1. For this system, experimental breakthrough curves were measured for tracer pulses migrating in a steady-state flow field through the column in two directions, from the fine segment to the coarse segment (FC direction), or from the coarse segment to the fine segment (CF direction). From the mild assumption of concentration and flux continuity across the interface, similar breakthrough curves in the FC and CF directions were intuitively expected because tracers experience equal lengths of subdomains in both directions. Interestingly, experiments revealed different behaviors of the breakthrough curves, with tracers migrating in the FC direction arriving

* Corresponding author. Tel.: +52 55 58044650; fax: +52 55 58044900.
E-mail address: levyinzunza@gmail.com (L. Inzunza).

http://dx.doi.org/10.1016/j.physa.2014.07.026
0378-4371/

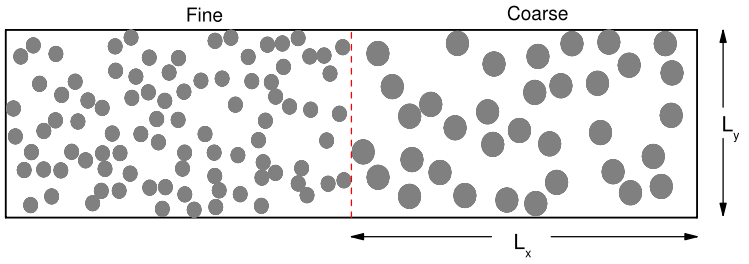

Fig. 1. Schematic description of the diffusion transport system. The coarse and the fine porous media have the same porosity.

significantly faster than in the CF direction. Besides, as the flow rate increased, the differences between the breakthrough curves diminished. It was argued that this transport asymmetry was indicating the significant, time-dependent tracer accumulation in the resident concentration profile across the heterogeneity profile. Berkowitz et al. [1] also showed that the use of conventional advection–dispersion equations is inadequate for describing the asymmetric behavior of the experimentally determined breakthrough curves. It was also argued that the resident concentration profile across the heterogeneity interface displays significant accumulation of tracers. Subsequently, Appuhamillage et al. [2] developed a Fickian theory for asymmetries (i.e., skewness) in breakthrough curves for transport across an interface. Cortis and Zoia [3] proposed a definition for the solute flux across sharp interfaces and explored the underlying microscopic particle dynamics by applying Monte Carlo simulation. Interestingly, the results were consistent with the findings reported by Berkowitz et al. [1] and explained the observed transport asymmetry.

The differences in the breakthrough curves reported by Berkowitz et al. [1] are induced by subtle transport effects, involving both advection and diffusion mechanisms. In particular, it is not clear whether the transport asymmetries are caused by local heterogeneities of the specific porous medium set-up. It is particularly important to remark that transport asymmetries are reduced as the flow-rate is increased. This suggests that differences in breakthrough curves are caused mainly by diffusion transport across the interface. Motivated by this, in the present work we study Berkowitz et al.'s set-up, by considering both diffusion and advection of tracers across an interface between two homogeneous porous media of the same porosity. Results derived from the simulation of Brownian tracers in random porous media show that, as observed in Berkowitz et al.'s experiments, tracers migrating in the FC direction arrive significantly faster than in the CF direction. A simple diffusion equation is used for explaining the transport asymmetries. In turn, it is shown that asymmetries are caused by a convection-like effect induced by sharp variations of effective diffusivity across the interface.

2. System description

As illustrated in Fig. 1, the system under consideration consists of two different 2D saturated porous media having the same porosity value ε_f (i.e., the area of the fluid contained in the porous medium relative to the total area as given by L_xL_y). The porous media are composed of non-overlapping circular obstacles randomly distributed. It should be noted that Fig. 1 is only a schematic diagram used for illustrative purpose. As will be specified in Section 3, the obstacle density used in experiments in Ref. [1] and numerical simulations in this work are significantly higher than that illustrated in Fig. 1. The diffusion transport is simulated by overdamped Brownian particles freely moving in the fluid and being reflected by the obstacles. The overdamped dynamics of the particles is modeled by the Langevin equation

$$\frac{\mathrm{d}\mathbf{r}}{\mathrm{d}t} = \sqrt{2D_0}\boldsymbol{\xi}(t) \tag{1}$$

where D_0 is the bulk diffusivity, $\mathbf{r} = (x, y)$ and $\boldsymbol{\xi}(t) = (\xi_x(t), \xi_y(t))$ are zero-mean white Gaussian noises with autocorrelation functions $\langle \xi_i(t), \xi_j(t') \rangle = \delta_{ij}\delta(t - t')$ with $i, j = x, y$. The well-known Milstein algorithm was used for numerical integration of Eq. (1). The value $D_0 = 1$ was used for all numerical simulations. The time step was set at $\Delta t = 10^{-5}$, so that $\sqrt{2D_0\Delta t} \ll 1$. That is, the mean path length is about 0.0044, which is sufficiently small for giving at least 225 steps before the tracers escape from the porous medium domain.

The motivation behind our work was the result in Berkowitz et al.'s experiments showing transport asymmetries in the axial direction. In fact, such experiments included both dispersion and convection mechanisms. The key observation in Berkowitz et al.'s paper is that the transport asymmetry was reduced as the mean flow velocity was increased. This suggested that diffusion might have an important role in the transport asymmetry. For exploring this idea, we designed the numerical experiment, based on Brownian particle simulations, described in our manuscript. It should be emphasized that our main intention was not to reproduce the specific physical conditions of Berkowitz et al.'s experiments, but rather to provide some exploratory insights on the origin of the experimental transport asymmetry. To this end, we maintained the system set-up as simple as possible for retaining the main characteristics necessary for exploring the effects of discontinuous porous media interface in the directional transport of Brownian particles. Finally, given that our analysis is not intended for the specific experimental conditions, the use of unit diffusion is a common practice in the numerical simulation of Brownian particles via the Langevin equation (1).

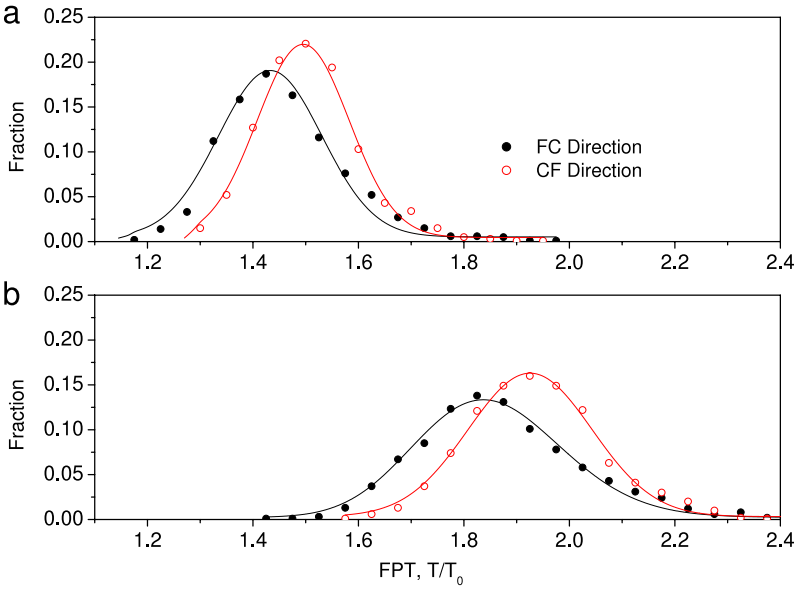

Fig. 2. Example of first passage time distributions for the FC and the CF transport directions. (a) $\varepsilon_f = 0.76$, (b) $\varepsilon_f = 0.68$. In both cases, $N_{\mathrm{Tr}} = 10{,}000$, $N_{\mathrm{PM}} = 1000$, $R_F = 0.02$ and $R_C = 0.0035$. For the sake of comparison, the continuous line is a Gaussian (normal) distribution.

For simulating tracer particles being transported along the composed porous medium, initial conditions are vertically and uniformly distributed along the entry boundary, corresponding to $x = -L_x$ (resp., $x = +L_x$) for diffusion transport in the FC direction (resp., in the CF direction). The entry boundary is set as reflecting, while the exit boundary as absorbing. The ratio between the crossing times between the two transport directions is considered as a diffusion asymmetry, which is quantified as

$$\alpha = \frac{\langle T_{\mathrm{CF}} \rangle}{\langle T_{\mathrm{FC}} \rangle} \tag{2}$$

where $\langle T_{\mathrm{CF}} \rangle$ and $\langle T_{\mathrm{FC}} \rangle$ are the mean first passage time (MFPT) in the CF and FC directions, respectively. In this way, values $\alpha \neq 1$ should indicate the presence of diffusion asymmetries in the transport of tracers across the interface. The MFPT was computed as follows:

(a) For a given porosity value ε_f, construct a random distribution of circular obstacles of radius R_F and R_C, with $R_F < R_C$, for the fine and coarse regions, respectively. Since the porosity is the same for the fine and coarse regions, one should have that $N_F R_F^2 = N_C R_F^2$, where N_F and N_C are the number of circular obstacles in the fine and coarse regions, respectively.
(b) For N_{Tr} tracers with initial conditions placed in the entry boundary, compute the first passage time as the time elapsed for reaching the exit boundary.
(c) For avoiding bias induced by a particular obstacles distribution, the above two steps are repeated over N_{PM} porous medium configurations obtained by randomly redistributing the obstacles in each region.
(d) Compute the MFPT by averaging over the N_{Tr} tracers and the N_{PM} porous medium configurations.

Intuitively, tracers have similar residence times in the fine and coarse regions. An interesting question is whether the interface has a direction-dependent effect in the transport of tracers across the system.

3. Results and discussion

The numerical computations were carried out for $L_y = 2$, $N_{\mathrm{Tr}} = 10{,}000$ and $N_{\mathrm{PM}} = 1000$. For a given porosity, this corresponds to the simulation of 10^7 trajectories for each transport direction (i.e., FC and CF directions). For $L_x = 1$, $R_F = 0.02$ and $R_C = 0.0035$, Fig. 2 presents two typical directional distributions of first passage times normalized by the obstacle-free first passage time $T_0 = L_x^2/2D_0 = 0.5$. The points in Fig. 2 represent the numerical results and the lines are used only for guiding the eye. The results in Fig. 2(a) correspond to the porosity value $\varepsilon_f = 0.76$, while the results in Fig. 2(b) correspond to $\varepsilon_f = 0.68$. Since $1 - \varepsilon_f = \frac{\pi R^2 N_{\mathrm{obs}}}{L_x L_y}$, where N_{obs} is the number of obstacles, the average density of obstacles $\frac{N_{\mathrm{obs}}}{L_x L_y}$ was about 190–250 and 1000–3000 for $R_F = 0.02$ and $R_C = 0.0035$, respectively. Similar qualitative results were obtained for other porosity values and other obstacle radius. As in the Berkowitz et al.'s experimental set-up, these parameters represent a composed porous medium with homogeneous porosity, but different obstacle radius. The main feature is the asymmetry of the first passage time distribution. In fact, one has that the transport asymmetry is $\alpha \approx 1.043$ and $\alpha \approx 1.056$, respectively.

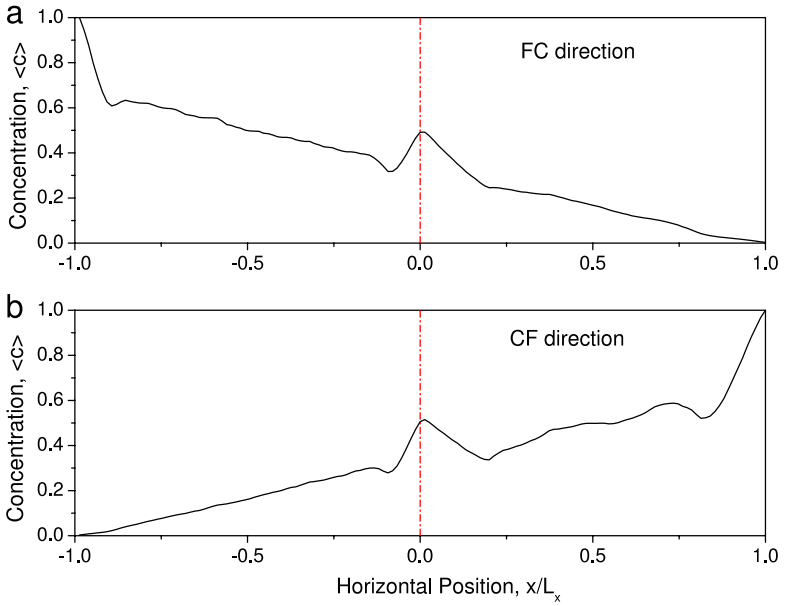

Fig. 3. Resident concentration profiles for $\varepsilon_f = 0.68$, $R_F = 0.02$ and $R_C = 0.0035$. The maximum at the interface location seems to indicate mass accumulation in the interface vicinity.

This means that, on the average, tracers took about 4%–6% more time for crossing in the CF direction than in the FC direction. For other porosity and radius values, we have found asymmetries as high as about 10%. The numerical results provided in Fig. 2 indicate that, despite the porosity equality between both porous media, diffusion transport asymmetries can arise as a consequence of asymmetries in the porous medium configuration. Certainly, the results in Fig. 2 are in agreement with the experimental results reported by Berkowitz et al. [1] for porous medium systems including saturating fluid flow. In this way, the results derived from Brownian tracer simulations indicate that diffusion effects can largely cause transport asymmetries across the porous media boundaries.

The previous numerical results indicate that transport of particles across heterogeneous interfaces can lead to asymmetric transport. This is reflected when tracers move faster in some directions where trajectories find reduced resistance. In fact, it has been shown that heterogeneous interfaces can induce an apparent drift or advection-like effect, which can be exploited for rectification of diffusive particles [4–6]. In fact, the asymmetry effect shares some similarities with biased Brownian motion in corrugated channels [7].

3.1. Resident concentration

Hornung et al. [8] employed Brownian particle tracking simulations for evaluating the discontinuity effects arising in terms of diffusive-only systems. The numerical results showed that mass can accumulate at the interface. Mass accumulation in the vicinity of the interface was evaluated by estimating the resident concentration. To this end, the average concentration of tracers along the horizontal coordinate was computed by dividing the system length $2L_x$ into N_s vertical strips of width Δx and counting the number of times the trajectories remain within a given vertical strip. Subsequently, the resulting profile was normalized with respect to the maximum value, which is located at the entry boundary. The porous medium length $L_x = 1$ was used for magnifying the effects at the interface. The results for $R_F = 0.02$, $R_C = 0.0035$ and $\varepsilon_f = 0.68$, are shown in Fig. 3, where the resident concentration profile was computed for $\Delta x = 0.01$ and averaged over $N_{\mathrm{Tr}} = 10{,}000$ tracer trajectories and $N_{\mathrm{PM}} = 1000$ random porous medium configurations. For both transport directions, the resident concentration profile exhibits a fast decrement at the entry boundary, which can be caused by local porous medium fluctuations. The most interesting feature is the presence of a concentration maximum in the interface vicinity, suggesting mass accumulation when Brownian tracers transit between the porous medium regions.

The resident concentration computed above corresponds to a concentration averaged over the control volume $V = L_y \Delta x$. That is, if c is the pointwise concentration of tracers moving in the saturating fluid and $\langle c \rangle$ is the resident concentration averaged over the volume V, then

$$\langle c \rangle = \frac{1}{V} \int_{V_f} c \mathrm{d}V \tag{3}$$

where $V_f = \varepsilon_f L_y \Delta x$ is the volume of the saturating fluid in the control volume $V = L_y \Delta x$. However, the averaged concentration $\langle c \rangle$ is computed relative to the whole volume V, including both saturating fluid and impermeable obstacles.

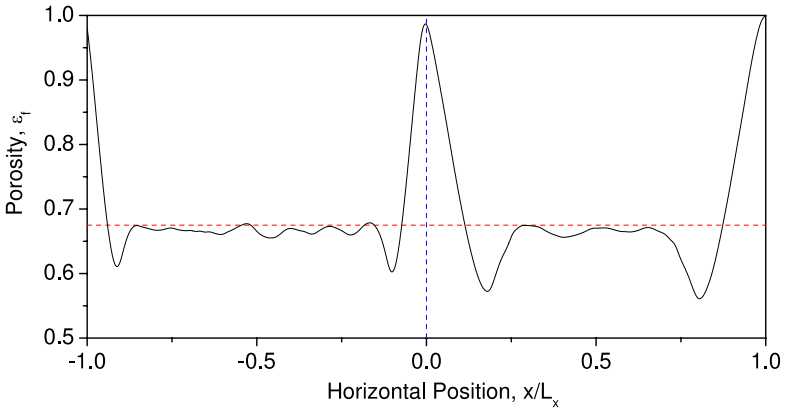

Fig. 4. Average spatial variations of porosity for the nominal porosity $\varepsilon_f = 0.68$, and obstacle radius $R_F = 0.02$ and $R_C = 0.0035$. The maximum at the interface is caused by the fine-to-coarse porous medium transition.

A more suitable form of averaged concentration should be computed in terms of the saturating fluid only; namely,

$$\langle c\rangle_f = \frac{1}{V_f}\int_{V_f} c_f \mathrm{d}V. \tag{4}$$

This concentration is commonly referred to as the intrinsic average concentration [9]. It is noted that the relation between these two concentrations is given by

$$\langle c\rangle = \varepsilon_f \langle c\rangle_f . \tag{5}$$

To discard the effects of local spatial variations of porosity in the resident concentration fluctuations, the intrinsic average concentration $\langle c\rangle_f$ should be computed. According to the expression given by Eq. (5), the spatial variations of porosity should be available. In this way, the variations of the porosity $\varepsilon_f(x)$ with respect to the horizontal coordinates were computed as follows. Similar to the procedure for resident computation estimation, the horizontal domain is divided into N_s vertical strips of width Δx. For each strip, the porosity is computed and averaged over N_{PM} porous media configurations. The porosity was evaluated by the hits of uniformly distributed random numbers over the vertical strips, and the corresponding porosity value was estimated as the fraction of hits over the saturating fluid for 10^6 trials. The procedure was checked against simple configurations with only one regular (e.g., square, circle, etc.) obstacle. Fig. 4 presents the average spatial variations of porosity, obtained from averaging over 10,000 configurations of the porous medium, for the nominal porosity $\varepsilon_f = 0.68$, and obstacle radius $R_F = 0.02$ and $R_C = 0.0035$. These parameters correspond to the resident concentration profile depicted in Fig. 3. In the porous medium bulk, the porosity exhibits small statistical fluctuations over the nominal value of $\varepsilon_f = 0.68$. However, boundary effects introduced positive departures from the porosity values near the boundaries $-L_x$ and $+L_x$. Interestingly, the interface where the two porous media configurations are coupled the porosity presents a nearly symmetric variation with the maximum at the interface location. One can use the estimated porosity profile for computing the intrinsic resident concentration as $\langle c\rangle_f = \langle c\rangle / \varepsilon_f$. Fig. 5 presents the profiles of the intrinsic resident concentration for both transport directions. After correcting by spatial porosity variations, the intrinsic concentration presents a monotonous behavior, without maximum values at the heterogeneous interface. That is, when expressed only with respect to the saturating fluid, the resident concentration does not reflect mass accumulation in a vicinity of the interface.

3.2. Effect of the channel length

Apparently, discontinuous effects at the porous media interface cause transport asymmetry. Here, particles undergo a change in the mean trajectory step as consequence of different mean distance between obstacles. In this way, it should be expected that the channel length has an important effect in the transport asymmetry as the relative effect of the interface is reduced as the channel length is increased. For obstacle radius $R_F = 0.02$ and $R_C = 0.0035$, Fig. 6 presents the effect of the channel length in the transport asymmetry for two different porosity values. The transport asymmetry ratio shows a gradual decrease as the channel length increases, indicating that the asymmetry is merely an effect of the porous medium interface. For large channel lengths, transport along the porous medium bulk dominates over the transient effect induced by discontinuity in the porous medium configuration.

3.3. Simple macroscopic modeling

It has been argued that the apparent mass accumulation at the heterogeneous interface (see Fig. 3) indicates that classical Fick's law cannot be applied for describing the diffusion transport in heterogeneous porous media. In fact, the presence of

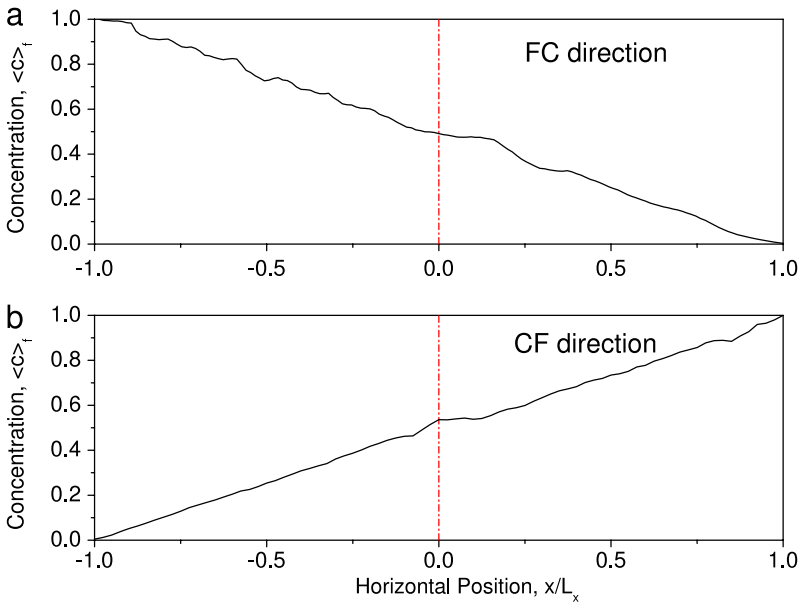

Fig. 5. Profiles of the intrinsic resident concentration $\langle c\rangle_f = \langle c\rangle/\varepsilon_f$. For both transport directions. After correcting by porosity variations, the resident concentration exhibits a monotonous behavior.

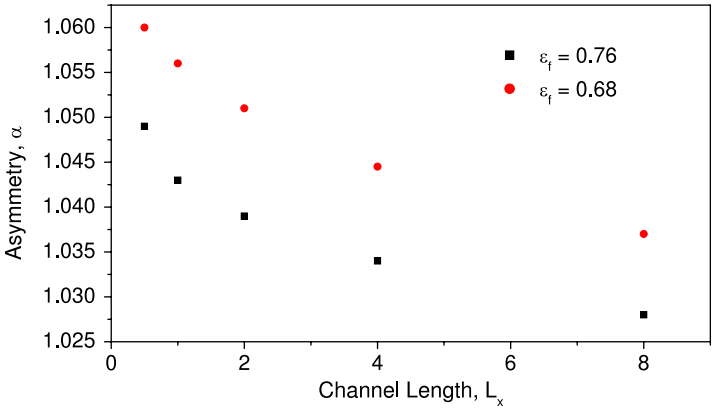

Fig. 6. Effect of the channel length in the transport asymmetry for two different porosity values.

a maximum of concentration at the interface would imply that mass could be transferred against concentration gradients. However, the results in Fig. 5 suggest that Fick's law can be used, but only when the physical modeling is based on the intrinsic resident concentration, $\langle c\rangle_f$. An interesting question is whether an effective medium modeling approach can account for the transport asymmetry across the interface. The diffusion equation with diffusivity depending on the horizontal position can be written as

$$\frac{\partial \langle c\rangle_f}{\partial t} = \frac{\partial}{\partial x}\left(D_{\text{eff}}(x)\frac{\partial \langle c\rangle_f}{\partial x}\right). \tag{6}$$

If one assumes that $D_{\text{eff}}(x)$ is a differentiable function, one has that Eq. (6) can be written as a diffusion–convection equation as follows:

$$\frac{\partial \langle c\rangle_f}{\partial t} = -v(x)\frac{\partial \langle c\rangle_f}{\partial x} + D_{\text{eff}}(x)\frac{\partial^2 \langle c\rangle_f}{\partial x^2} \tag{7}$$

where $v(x) = -\mathrm{d}D_{\text{eff}}/\mathrm{d}x$. Interestingly, spatial variations of effective diffusivity can induce a convection-like effect. A positive (resp., negative) diffusivity gradient induces a negative (resp., positive) velocity. In this way, tracers moving against diffusivity gradients perceive a positive driving force, while tracers moving along diffusivity gradients are subjected to a negative driving force. This suggests that transport asymmetry across a heterogeneous interface can be caused by spatial variations of effective diffusivity. For evaluating this potential effect, Eq. (6) was numerically solved for a two-domain system

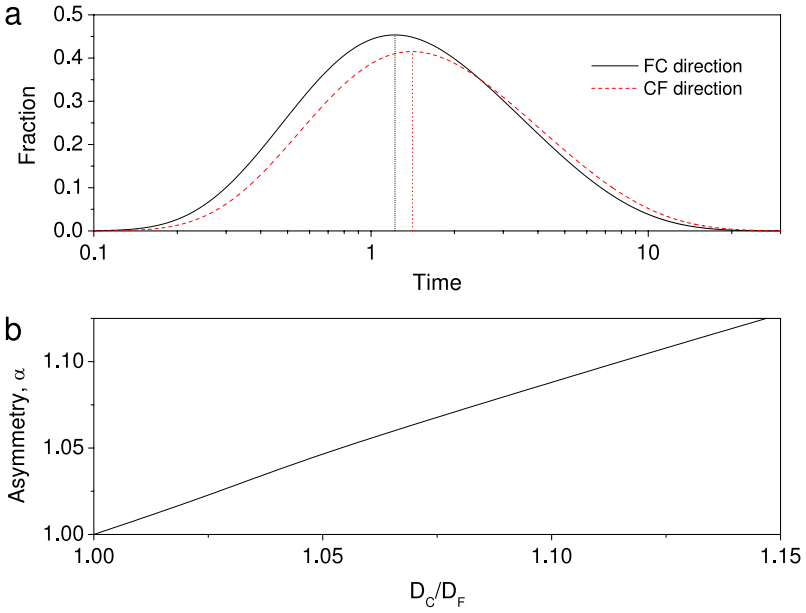

Fig. 7. (a) Breakthrough curves obtained for model simulation with $D_C/D_F = 1.05$. (b) Diffusion asymmetry as function of the diffusivity ratio D_C/D_F. The points represent results from numerical simulation of Brownian tracers.

similar to that in Fig. 1. Here, the fine and coarse sub-regions are considered as homogeneous domains with diffusivity D_F and D_C, respectively. For avoiding numerical instabilities induced by discontinuous parameter at the interface, the diffusivity change from fine to coarse regions was smoothed by adjusting to the Boltzmann (sigmoid) function. Central finite-differences were used for discretization of the diffusion operator in the right-hand side of Eq. (6). For simulating the breakthrough curve obtained by Brownian particle simulation, an initial amount of tracers was placed at the entry boundary (either $x = -L_x$ and $x = +L_x$), while the full domain was emptied. Reflecting condition (i.e., $d\langle c\rangle_f/dx = 0$) was imposed at the entry boundary. For $L_x = 1.0$, $D_F = 1.0$ and $D_C = 1.05$, Fig. 7(a) presents the breakthrough for the FC and CF directions. Similar to the results in Fig. 2, the behavior of the breakthrough curve depends on the transport direction, with tracers moving faster in the FC direction than in the CF direction. Vertical dotted lines highlight the position of the maximum. The asymmetry, quantified by Eq. (2) is about 1.05. Fig. 7(b) shows that the diffusion asymmetry is an increasing function of the diffusivity ratio D_C/D_F. That is, the higher the diffusivity changes at the interface, the higher the diffusion asymmetry.

3.4. Effective diffusivity

The previous results indicate that diffusivity change at the heterogeneous interface can induce diffusion asymmetry, with preferred transport in the direction where diffusivity changes from lower to higher values. Effective diffusivity differences in the heterogeneous medium schematized in Fig. 1 are not caused by porosity differences since both fine and coarse regions have the same value. Recall that the effective diffusivity of porous media can be expressed as

$$D_{\text{eff}} = \frac{\varepsilon_f D_0}{\tau} \tag{8}$$

where τ is the tortuosity. It should be mentioned that the concept of porosity is dependent on the application [10,11]. In the classical definition of effective diffusivity given by Eq. (8), tortuosity is referred to as diffusion tortuosity but other definitions can arise depending on the transport situation. In this way, for a given porosity ε_f, the effective diffusivity decreases when the tortuosity increases. Regarding the heterogeneous porous medium considered in this work (Fig. 1), the fine region retains the same porosity value than the coarse medium at the expense of a higher number of obstacles. Intuitively, a larger number of obstacles within the same region should increase the tortuosity and, hence, reduce the effective diffusivity. Eq. (8) was used for estimating the tortuosity differences between coarse and fine sections of the porous medium. To this end, the following procedure was used: for a given porosity ε_f, tortuosity differences between fine and coarse regions were estimated by using Eq. (8) written in the form $\tau = \frac{\varepsilon_f D_0}{D_{\text{eff}}}$. For using this equation, one should dispose of the effective diffusivity for each porous medium region. To this end, the effective diffusivity was estimated along the following steps: (a) Fix a porosity value, ε_f. (b) Over a square domain of length $L_{\text{PM}} = 100$, as done for the heterogeneous porous media, construct a homogeneous porous medium with obstacles of radius R. For maintaining the average porosity fixed, the number of obstacles should meet the constraint $1 - \varepsilon_f = \frac{\pi R^2 N_{\text{obs}}}{L_{\text{PM}}^2}$. (c) Undergo Brownian trajectories over many trajectories ($N_{\text{Tr}} = 10{,}000$) and diverse porous

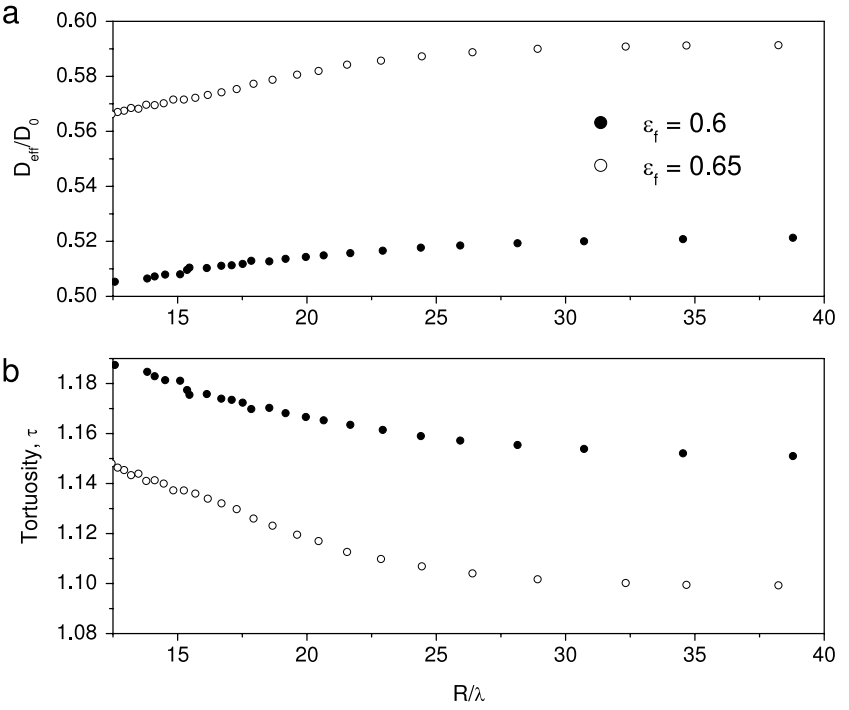

Fig. 8. (a) Effective diffusivity as function of the obstacle radius for two different porosity values. The effective diffusivity decreases as the obstacle radius is reduced. (b) Tortuosity is estimated from the effective diffusivity profile by using the classical expression $D_{\text{eff}}/D_0 = \varepsilon_f/\tau$.

medium configurations ($N_{\text{PM}} = 1000$) for computing the mean square displacement (MSD) $\langle x(t)^2 \rangle$. Since the porous medium is homogeneous, the coordinate x can be chosen as the horizontal direction. (d) The effective diffusivity D_{eff} as $\langle x(t)^2 \rangle / t$ for sufficiently large time t. That is, by plotting the MSD against time, the effective diffusivity is computed as the slope of the curve for sufficiently large times [12]. (e) Estimate the porous medium tortuosity according to the equation $\tau = \frac{\varepsilon_f D_0}{D_{\text{eff}}}$. For a fixed porosity value, ε_f, the application of the above procedure leads to the estimated tortuosity as function of the porous medium radius, R.

For two different porosity values, Fig. 8(a) presents the effective diffusivity as function of the obstacle radius, R, normalized by the mean path length, λ, of the Brownian tracers. That is, $\lambda = \sigma\sqrt{2D_0\Delta t}$, where Δt is the time step and σ is the standard deviation of the Gaussian random number generator. In our case, $\Delta t = 10^{-5}$, $\sigma = 1.0$ and $D_0 = 1.0$, so that $\lambda = 4.47 \times 10^{-2}$. Interestingly, the estimated effective diffusivity decreases for smaller obstacle radius. This indicates that subtle differences of effective diffusivity between fine and coarse porous medium configurations are introduced by tortuosity differences. Given the effective diffusivity in Fig. 8(a), (b) presents the tortuosity, computed with the equation $\tau = \frac{\varepsilon_f D_0}{D_{\text{eff}}}$, as function of the obstacle radius for the same porosity values used in Fig. 8(a). It is noted that, as expected, tortuosity increases for finer porous medium configurations. The results in Figs. 7 and 8 suggest that the differences of the breakthrough curves for the diffusion transport system schematized in Fig. 1 can be largely explained by small diffusivity differences. In turn, given that the porosity is constant; such diffusivity differences are introduced by configuration differences (i.e., tortuosity) between fine and coarse porous media.

3.5. Extended Fick–Jacobs predictions

The results in Fig. 8 suggested that the transport asymmetry could be caused by subtle differences in the effective diffusivity, which can be attributed to tortuosity differences between coarse and fine regions. However, Fig. 4 showed important porosity variations in a vicinity of the porous medium interface. An analogy between the porous medium system in Fig. 1 and a channel with width variations can be made as follows. In the latter case, the 1D concentration can be described by the extended Fick–Jacobs equations (eFJ), which is obtained from projecting the corresponding 2D transport equation along the horizontal direction [13,14]. Specifically, the eFJ equation can be written as follows:

$$\frac{\partial \langle c \rangle_f}{\partial t} = \frac{\partial}{\partial x}\left(D_{\text{eff}}(x) A(x) \left(\frac{\partial}{\partial x} \frac{\langle c \rangle_f}{A(x)} \right) \right) \tag{9}$$

where $A(x)$ is the channel width. The porous medium systems can be seen as a channel described by the eFJ equation if the channel width $A(x)$ is taken as the porosity $\varepsilon_f(x)$. In such case, the estimated porosity profile, similar to the one shown

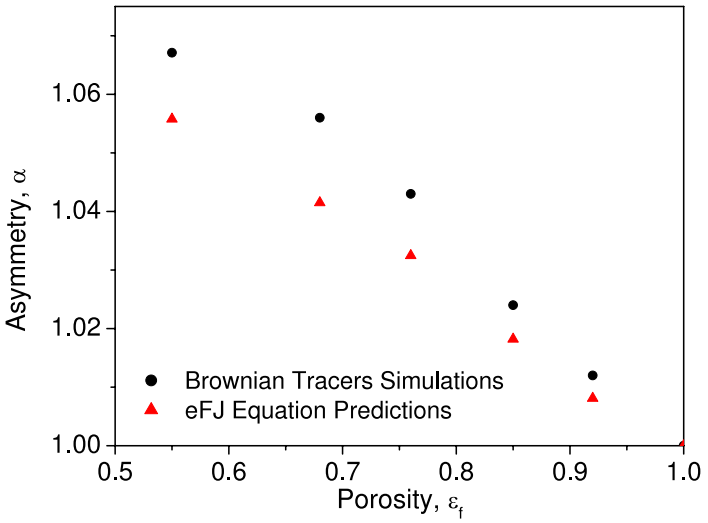

Fig. 9. Comparison between Brownian tracers simulations and predictions obtained from the extended Fick–Jacobs equation.

in Fig. 4, can be used in Eq. (9). Regarding the effective diffusivity, some expression has been proposed in the literature. A commonly used expression for $D_{\text{eff}}(x)$ is the Reguera and Rubi's expression [15]:

$$D_{\text{eff}}(x) = \frac{D_0}{\left(1 + \frac{A'(x)^2}{4}\right)^{1/3}}. \tag{10}$$

A numerical scheme similar to the one used for simulating Eq. (7), was used for solving numerically Eq. (9). The equivalence $A(x) = \varepsilon_f(x)$ was taken, and the effective diffusivity was estimated from Eq. (10). As made for the profile exhibited in Fig. 4, the position-dependent porosity was obtained by averaging over 10,000 porous medium random configurations. Cubic splines were used for interpolating the porosity profile. For $R_F = 0.02$ and $R_C = 0.0035$, Fig. 9 compares the predictions obtained from the eFJ equation and the numerical simulations with Brownian tracers simulations. The transport asymmetries predicted by the eFJ equation are induced by porosity asymmetries in the interface vicinity (see Fig. 4). However, the predictions made by the eFJ equation are smaller than those obtained with the simulations of Brownian tracers. Maybe, the overall transport asymmetries observed in Brownian tracer simulations are caused by the combination of subtle porosity and effective diffusivity (as caused by tortuosity differences) differences. The model given by Eq. (9) provides a good, although lower prediction of the transport asymmetry. The discrepancies could be also attributed to the porosity fluctuations that were not considered in the solution of Eq. (9).

3.6. Effect of a constant driving force

In the experiments of Berkowitz et al., it was observed that the transport asymmetry exhibited a decreasing trend as the fluid velocity was increased. For exploring this effect from our numerical simulations framework, an external force $\mathbf{F} = (F_x, 0)$ acting on the tracers was added to the Langevin equation (1). In this way, one has that the tracers dynamics are governed by

$$\frac{d\mathbf{r}}{dt} = \mathbf{F} + \sqrt{2D_0}\boldsymbol{\xi}(t). \tag{11}$$

In terms of a macroscopic transport equation, the force $\mathbf{F} = (F_x, 0)$ has the effect of a constant velocity along the x-direction [16]. For $R_F = 0.02$ and $R_C = 0.0035$, Fig. 10 exhibits the transport asymmetry as function of the force F_x, for two different porosity values. It is noted that, as in experiments, the transport asymmetry is decreased as the force is increased. This result supports our claim that the transport asymmetry reported in Ref. [1] has its origins in diffusion effects about the transport medium interface.

4. Conclusions

Numerical simulations of Brownian tracers moving across a heterogeneous interface of porous media have shown that the behavior of the breakthrough curves is direction-dependent. In fact, the results in this work provide important insights for interpreting the findings of previously published experimental results showing that tracers move faster in the fine-to-coarse direction than in the opposite. Numerical solution of the diffusion equation and the extended Fick–Jacobs equation

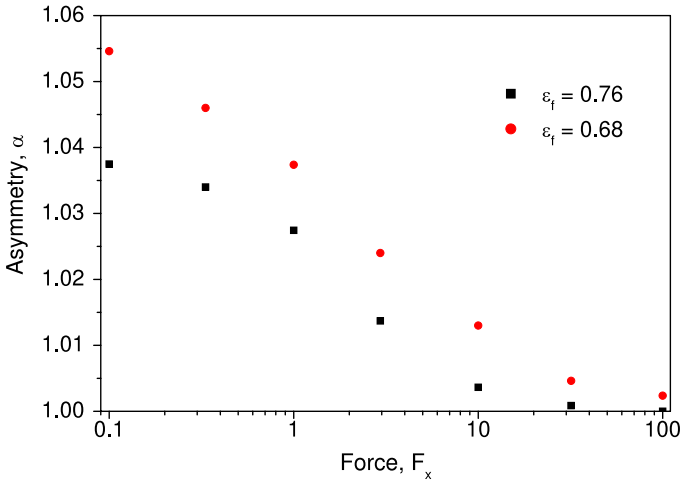

Fig. 10. Transport asymmetry as function of an added force in the direction of the diffusion transport. Here, $R_F = 0.02$ and $R_C = 0.0035$.

suggested that changes of effective diffusivity and porosity at the interface could cause transport asymmetry of the type obtained with experiments and simulation of Brownian tracers. Within this rationale, it was shown that, for a given porosity value, the tortuosity of the porous medium has a negative effect in the effective diffusivity.

References

[1] B. Berkowitz, A. Cortis, I. Dror, H. Scher, Laboratory experiments on dispersive transport across interfaces: the role of flow direction, Water Resour. Res. 45 (2009) W02201. http://dx.doi.org/10.1029/2008WR007342.
[2] T.A. Appuhamillage, V.A. Bokil, E. Thomann, E. Waymire, B.D. Wood, Solute transport across an interface: a Fickian theory for skewness in breakthrough curves, Water Resour. Res. 46 (2010) W07511. http://dx.doi.org/10.1029/2009WR008258.
[3] A. Cortis, A. Zoia, Model of dispersive transport across sharp interfaces between porous materials, Phys. Rev. E 80 (2009) 011122.
[4] P. Lancon, G. Batrouni, L. Lobry, N. Ostrowsky, Drift without flux: Brownian walker with a space-dependent diffusion coefficient, Europhys. Lett. 54 (2001) 28–34.
[5] P.F. Tupper, X. Yang, A paradox of state-dependent diffusion and how to solve it, Proc. R. Soc. A 468 (2012) 3864–3881.
[6] F. Marchesoni, Drift in diffusion gradients, Materials 6 (2013) 3598–3609.
[7] S. Martens, G. Schmid, L. Schimansky-Geier, P. Hänggi, Biased Brownian motion in extremely corrugated tubes, Chaos 21 (2011) 047518.
[8] G. Hornung, B. Berkowitz, N. Barkai, Morphogen gradient formation in a complex environment: an anomalous diffusion model, Phys. Rev. E 72 (2005) 041916.
[9] S. Whitaker, The Method of Volume Averaging, Kluwer Academic Publishers, Dordrecht, 1999.
[10] M.B. Clennell, Tortuosity: a guide through the maze, Geol. Soc., Lond., Spec. Publ. 122 (1997) 299–344.
[11] F.J. Valdes-Parada, M.L. Porter, B.D. Wood, The role of tortuosity in upscaling, Transp. Porous Media 88 (2011) 1–30.
[12] A.M. Berezhkovskii, L. Dagdug, S.M. Bezrukov, Discriminating between anomalous diffusion and transient behavior in microheterogeneous environments, Biophys. J. 106 (2014) L09–L11.
[13] R. Zwanzig, Diffusion past an entropy barrier, J. Phys. Chem. 96 (1992) 3926–3930.
[14] P. Kalinay, J.K. Percus, Corrections to the Fick–Jacobs equation, Phys. Rev. E 74 (2006) 041203.
[15] D. Reguera, J.M. Rubi, Kinetic equations for diffusion in the presence of entropic barriers, Phys. Rev. E 64 (2001) 061106.
[16] H. Risken, The Fokker–Planck Equation, second ed., Springer, Berlin, 1989.